SHOCK MOVEMENTS IN TRANSONIC FLOW AROUND A RECTANGULAR WING SECTION

Jörgen Held*
Dept. of Heat and Power Engineering/Fluid Mechanics,
Lund Institute of Technology, SE-221 00 Lund, Sweden

Laszlo Fuchs†
Dept. of Heat and Power Engineering/Fluid Mechanics,
Lund Institute of Technology, SE-221 00 Lund, Sweden

ABSTRACT

This is a phenomenological study of the interaction between a shock and a separated boundary layer using Large Eddy Simulation (LES). The geometry is the NACA 0012 profile. The computational Mach number is 0.799 and the angle of attack is 2.26 degrees. The simulations are done at different Reynolds numbers, $3 \cdot 10^5$, $5 \cdot 10^5$ and $1 \cdot 10^6$. The subgrid-scale (SGS) effect are accounted for through the inherent dissipation of the numerical algorithm and an anisotropic dynamic divergence subgrid-scale model (DDM). The amplitude and the frequency of the shock movements are reported. It is found that the DDM is too active in the region where the shock is located giving rise to an overestimate of SGS-turbulence. There is a certain periodicity in the shock movements. One of the dominating frequencies is shown to be related to the late stage of the transition process.

INTRODUCTION

For design and performance purposes it is important to understand how the shock interacts with the boundary layer. Therefore it is of interest to predict not only the mean location of the shock but also with which frequency and amplitude it moves around its mean position. If the shock is strong enough the flow separates due to the adverse pressure gradient. The pressure inside the separated region is higher than for attached flow. The separation also increases the drag. Hence, movements of the shock will affect the lift coefficient and the drag coefficient. The operating range of a wing is given by these two coefficients and the fuel consumption is directly related to the drag. The main problems associated with separated transonic flows are due to difficulties in modelling the turbulence in and near separated regions, determining the location of transition (Wilcox 1993) and determining accurately the shock location. Dynamic large eddy simulations have the potential to handle these problems (Germano et al. 1991). The flow under consideration is highly anisotropic. The proximal wall region of turbulence in boundary layer flows is anisotropic due to the constraint a wall imposes on the flow. The flow in the vicinity of the shock will also experience anisotropy. Subgrid-scale models with only one model parameter implicitly assume isotropy in the subgrid-scales. This problem is less pronounced if the flowfield is well resolved because the scales become more and more isotropic with higher wave number. The resolution requirement may be eased using a model which admits anisotropy in the subgrid-scales. Held and Fuchs (1997) developed such a model, the dynamic divergence model (DDM). The DDM contains three parameters, one in each spatial direction, admitting anisotropic turbulent viscosity.

FORMULATIONS

The governing equations for turbulent flows are the Navier-Stokes equations, mass and energy balance equations together with an equation of state. In large eddy simulations of turbulent flows, each variable in the flow domain, D, can be decomposed into a large scale component and a subgrid-scale component. This

*Ph.D. student
†Professor

is obtained by filtering the flow variable such that

$$\phi(\mathbf{x},t) = \overline{\phi}(\mathbf{x},t) + \phi'(\mathbf{x},t) \tag{1}$$

and

$$\overline{\phi}(\mathbf{x},t;\Delta) = \int_D \overline{G}(\mathbf{x}-\mathbf{x}';\Delta)\phi(\mathbf{x}',t)d^3\mathbf{x}' \tag{2}$$

where $\overline{\phi}$ is the large scale component, ϕ' is the subgrid-scale component, $\overline{G}(\mathbf{x}-\mathbf{x}';\Delta)$ is the filter function and Δ is the filter width, normally taken as the grid size. By using density weighted space averages, defined in an analogous manner to the Favre time average, the governing equations in Cartesian coordinates can be written as

Continuity

$$\frac{\partial \overline{\rho}}{\partial t} + \frac{\partial \overline{\rho}\widetilde{u_j}}{\partial x_j} = 0, \tag{3}$$

Momentum

$$\frac{\partial \overline{\rho}\widetilde{u_i}}{\partial t} + \frac{\partial \overline{\rho}\widetilde{u_i}\widetilde{u_j}}{\partial x_j} = -\frac{\partial \overline{p}}{\partial x_i} + \frac{\partial \overline{\sigma}_{ij}}{\partial x_j} + \frac{\partial \tau_{ij}}{\partial x_j} \tag{4}$$

Energy

$$C_p\left(\frac{\partial \overline{\rho T}}{\partial t} + \frac{\partial \overline{\rho u_i T}}{\partial x_i}\right) = \frac{\partial \overline{p}}{\partial t} + \overline{u_i \frac{\partial p}{\partial x_i}} + \overline{\Phi} + \frac{\partial}{\partial x_i}\left(k\overline{\frac{\partial T}{\partial x_i}}\right) \tag{5}$$

where u_j are the Cartesian velocity components, σ_{ij} is the molecular stress tensor, C_p is the specific heat at constant pressure, Φ is the viscous dissipation and k is the thermal conductivity. Here, C_p is assumed to be constant. The last term on the righthand side of the momentum equations is the divergence of the subgrid-scale stress tensor.

$$\frac{\partial \tau_{ij}}{\partial x_j} = \frac{\partial \overline{\rho}\widetilde{u_i}\widetilde{u_j}}{\partial x_j} - \frac{\partial \overline{\rho}\widetilde{u_i u_j}}{\partial x_j} \tag{6}$$

Dynamic Divergence Model (DDM)

Following Germano (1991) a test filter is introduced. The test filter width should exceed the grid filter width. A relation for the resolved turbulent stress, i.e. the turbulent scales between the two filter levels, can be explicitly expressed. This relation is called the Germano identity.

$$L_{ij} = T_{ij} - \widehat{\tau}_{ij} \tag{7}$$

Test filtered variables are denoted by a caret, ($\widehat{\ }$). The model parameters in the DDM are obtained by applying the divergence operator to the Germano identity. In this way the three model parameters are expressed directly and independently. Using the divergence operator to contract the expression for the resolved turbulent stress is a natural choice since it is the divergence of the subgrid-scale stress which enters into the momentum equations for the motion of the resolved scales.

$$\frac{\partial L_{ij}}{\partial x_j} = \frac{\partial T_{ij}}{\partial x_j} - \frac{\partial \widehat{\tau}_{ij}}{\partial x_j} = -\frac{\partial\{\widehat{\overline{\rho}}(\widehat{\widetilde{u_i}\widetilde{u_j}} - \widehat{\widetilde{u}}_i\widehat{\widetilde{u}}_j)\}}{\partial x_j} \tag{8}$$

The divergence of the subgrid-scale stress and the subtest filter stress are modelled by taking the divergence of the compressible generalisation of the Smagorinsky model (Erlebacher et al., 1990).

$$\frac{\partial \tau_{ij}}{\partial x_j} = C^{(i)}\frac{\partial\{2\Delta^2\overline{\rho}II_{\tilde{S}}^{1/2}(\tilde{S}_{ij} - \frac{1}{3}\tilde{S}_{kk}\delta_{ij})\}}{\partial x_j} = C^{(i)}\frac{\partial \alpha_{ij}}{\partial x_j} \tag{9}$$

and

$$\frac{\partial T_{ij}}{\partial x_j} = C^{(i)}\frac{\partial\{2\widehat{\Delta}^2\widehat{\overline{\rho}}II_{\widehat{\tilde{S}}}^{1/2}(\widehat{\tilde{S}}_{ij} - \frac{1}{3}\widehat{\tilde{S}}_{kk}\delta_{ij})\}}{\partial x_j} = C^{(i)}\frac{\partial \beta_{ij}}{x_j} \tag{10}$$

Note that no summation over the superscript, (i), is carried out. The three model parameters, $C^{(i)}$, are calculated during the simulation from the instantaneous flow field by combining Eq.s (8) - (10).

$$C^{(i)} = \frac{\partial L_{ij}/\partial x_j}{\partial \beta_{ik}/\partial x_k - \partial \widehat{\alpha}_{il}/\partial x_l} \tag{11}$$

To avoid unphysical values the model parameters $C^{(i)}$ are set to zero if $||\partial L_{ij}/\partial x_j|| < \epsilon$, where ϵ is a small value related to the numerical accuracy of the computed results. i.e. the model parameters are forced to be zero if there is no resolved turbulence. This is consistent with the assumption of scale-similarity of the turbulent stresses which the Germano identity is based on.

NUMERICAL METHODS

The calculations are performed with a finite volume based Navier-Stokes solver for general structured multiblock meshes. The scheme is based on a central formulation with second and fourth order dissipation terms. The discretisation, both in time and space, is of second order. An implicit time marching procedure is employed (Eliasson and Nordström, 1995).

Boundary Conditions

Riemann invariants are used as farfield boundary conditions (Hirsch, 1990). Periodic conditions are imposed in the spanwise direction. A no-slip condition is imposed on the wing surface. To resemble the experiment conducted by Harris (1981) a disturbance was introduced at $X/C = 0.05$ by adding a source term in

the momentum equations. The source term may be regarded as "numerical grains".

SIMULATIONS

Large eddy simulations of transonic flow around a rectangular wing section (NACA 0012) are investigated. An implicit SGS-model, where the subgrid-scale effect is implicitly accounted for through the inherent dissipation of the numerical algorithm, and the DDM are employed in this paper. The following simulations have been carried out

- $Re = 3 \cdot 10^5$, Implicit
- $Re = 3 \cdot 10^5$, DDM
- $Re = 5 \cdot 10^5$, Implicit
- $Re = 1 \cdot 10^6$, Implicit

The pressure distributions are compared with experimental data obtained by Harris (1981) for a Reynolds number of $3 \cdot 10^6$.

The Grid

The grid is a body-fitted C-mesh with 257x57x9 nodepoints in the streamwise, normal and spanwise direction respectively. The strecthing factor in the normal direction to the wing is 1.12.

Bounds

To ensure numerical stability the model parameters have to be bounded. Olsson and Fuchs (1994) investigated different local bounds. Based on their work the artificial bounds were initially calculated as follows.

$$\frac{-0.01}{Re} \leq C^{(i)} \leq \frac{0.5}{Re} \tag{12}$$

where Re is the Reynolds number based on the chord length and freestream values. However, due to stability problems the lower bound was changed to $-0.0025/Re$ indicating that the numerical value of the bound is *ad hoc*. Note that negative values of the model parameters imply back-scatter of energy from the subgrid-scales to the resolved scales. The upper bound is purely numerical and depends on the timestep.

RESULTS

Fig. 1 and 2 show the mean pressure coefficient distribution and the mean skin friction coefficient distribution respectively. The flow under consideration is highly Reynolds number dependent in the range investigated here. In fact Held and Fuchs (1998) showed that as the the Reynolds number was increased the position of the shock approached the experimental value obtained by Harris (1981). Held and Fuchs (1998) also showed that the flow is more or less inviscid upstream of the shock. The laminar boundary layer separates due to the strong shock on the upper surface. Further downstream the boundary layer reattaches and undergoes transition to turbulence. Notable is the discrepancy of the predicted pressure coefficient and skin friction calculated with the DDM and the implicit model at the position of the shock.

RMS of the fluctuating pressure coefficient and skin friction coefficient are shown in Fig. 3 and 4, respectively. Note that the skin friction coefficient and RMS of the skin coefficient fluctuations will decrease with increasing Reynolds number (decreasing viscosity). The peak in the RMS of $C_F{}'$ at $X/C = 0.05$ is due to the forced disturbance. The second peak is a result of shock wave movements. The RMS values indicate that the separated region behind the shock is laminar. Thereafter the RMS values increase due to transition/turbulence.

In order to follow the position of the shock the point most upstream and closest to the surface fulfilling a supersonic Mach number upstream and a subsonic downstream is traced. This point is obtained through linear interpolation. Fig. 5 shows the instantaneous Mach iso-contours for a Reynolds number of $3 \cdot 10^5$ calculated with the implicit model. There is no distinct shock wave. Part of the "main" shock is released as shocklets interacting with the boundary layer while travelling downstream. Due to difficulties in defining the shock wave at a Reynolds number of $3 \cdot 10^5$, the shock wave movements are calculated only for the higher Reynolds number where the shock is more distinct. The Fast Fourier Transform (FFT) of the shock movements for a Reynolds number of $5 \cdot 10^5$ and $1 \cdot 10^6$ are shown in Fig. 6 and 7 respectively. There is a certain periodicity in the shock movements. The dominating frequencies are around 40 Hz and 455 Hz for Reynolds number of $5 \cdot 10^5$. For Reynolds number $1 \cdot 10^6$ the dominating frequencies are around 35 Hz and 455 Hz with harmonics.

For Reynolds number $5 \cdot 10^5$ the mean position of the shock is at $X/C = 0.14$ and for Reynolds number $1 \cdot 10^6$ at $X/C = 0.22$. The RMS of the amplitude of the shock movements is only 2.7 per cent of the chord length in both cases. However, the maximum amplitude is as large as 10 per cent of the chord length in both cases.

Fig. 8 shows the kinetic energy of the fluctuations as a function of frequency at $X/C = 0.5$ which correspond to the point where the RMS of C_P' and C_F' increase rapidly. The late stage of the transition is associated with growth of fluctuations of frequencies around 450-550 Hz. Fig. 9 shows the kinetic energy of the fluctuations at $X/C = 0.6$. Note the amplification and that all frequencies are present. The energy spectrum of the turbulent kinetic energy at $X/C = 0.6$ for a Reynolds

number of $5 \cdot 10^5$ is shown in Fig. 10. The Kolmogorov -5/3 decay is also depicted. The resolved inertial subrange is contained within one decade of frequencies.

CONCLUSIONS AND DISCUSSION

The DDM affects mean properties such as mean C_P and mean C_F at the position of the shock. This indicates that the model is active in this region, giving rise to unreasonbly large SGS-turbulence. Of course, the whole idea of SGS-stress tensor having an asymptotically decaying (as a function of wave length) is incorrect near/across shocks. In fact the assessment of the SGS effects by using double filters is possible only when the resolved scales are filter-independent, which is not the case near the shock. The calculations here, are aimed at pointing out this difficulty. The bounds in the present form are user input and hence *ad hoc*. The following modifications of the model are considered. The pressure switch used for the second order numerical viscosity term may be used to avoid filtering close to the shock. The lower bound will also be modified. One suggestion is that the total dissipation (molecular, subgrid-scale and numerical dissipation) should be positive (Olsson and Fuchs, 1994).

The shock boundary layer interaction is extremely complex at the lower Reynolds number investigated here. There is no real distinct shock wave. Shocklets are released from the "main" shock. The shocklets interact with the boundary layer while travelling downstream. At higher Reynolds number the shock is more pronounced.

There is a certain periodicity in the shock movements. One of the dominating frequencies (455 Hz) is related to the late stage of the transition process. However, it's not clear if the shock movements trigger the transition or the other way around.

Even if the RMS value of the amplitude of the shock movements is small the maximum amplitude is large.

ACKNOWLEDGEMENT

We would like to thank Peter Eliasson and Ingemar Lindblad at the Aeronautical Research Institute of Sweden for providing the original EURANUS code. Computer resources from LUNARC at Lund University are greatfully acknowledged.

REFERENCES

Eliasson, P. and Nordström, J., 1995, " The Development of an Unsteady Solver for Moving Meshes", *FFA TN 1995-39*, The Aeronautical Research Institute of Sweden.

Erlebacher, G., Hussaini, M.Y., Speziale, C.G. and Zang, T.A., 1990, "Toward the large-eddy simulation of compressible flows, *ICASE Report, 90-76.*

Germano, M., Piomelli, U., Moin, P. and Cabot, W., 1991, "A dynamic subgrid-scale eddy viscosity model", *Phys. Fluids A*, **3**, pp. 1760-1765.

Harris, C.D., 1981, "Two-Dimensional Aerodynamic Characteristics of the NACA 0012 Airfoil in the Langley 8-foot Transonic Pressure Tunnel", *NASA, TM-81927.*

Held, J. and Fuchs, L., 1997, "Large Eddy Simulation of Compressible Separated Flow Around a NACA 0012 Wing Section", *AIAA paper No. 97-1931.*

Held, J. and Fuchs, L., 1998, "Large Eddy Simulation of Separated Transonic Flow Around a Wing Section", *AIAA paper No. 98-0405.*

Hirsch, C., 1990, "Numerical Computation of Internal and External Flows", *John Wiley & Sons.*

Olsson, M. and Fuchs, L.,1994, "Significant terms in dynamic SGS-modeling", In *Direct and large-eddy simulation I*, P.R. Voke, L. Kleiser and J-P. Chollet (Eds.), Netherlands. Kluwer Academic Publishers.

Wilcox, D.C., 1993, "Turbulence modeling for CFD", DCW Industries.

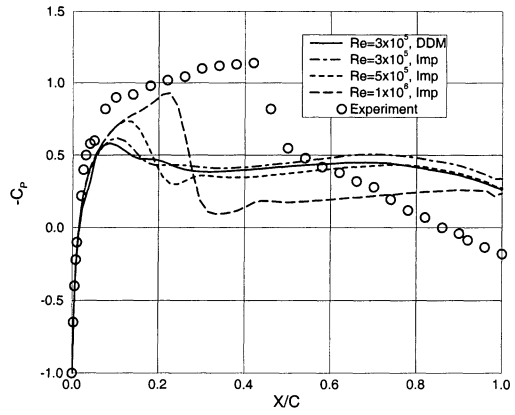

Figure 1: The chordwise pressure distribution on the upper surface.

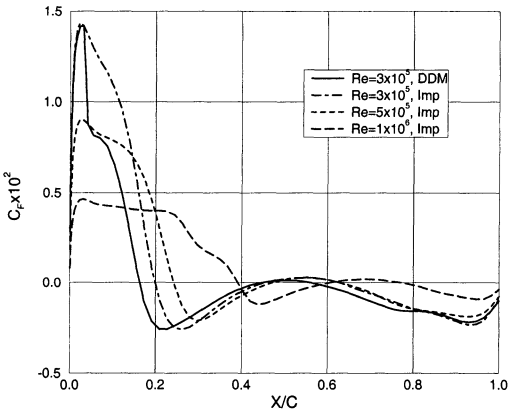

Figure 2: The chordwise skin friction coefficient distribution on the upper surface.

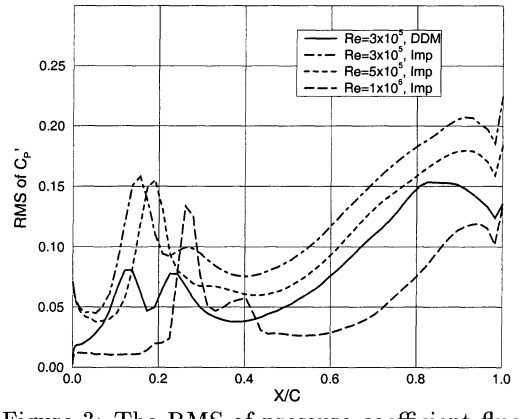

Figure 3: The RMS of pressure coefficient fluctuations on the upper surface.

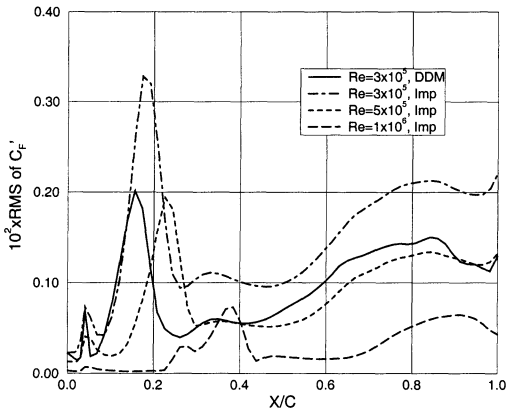

Figure 4: The RMS of skin friction coefficient fluctuations on the upper surface.

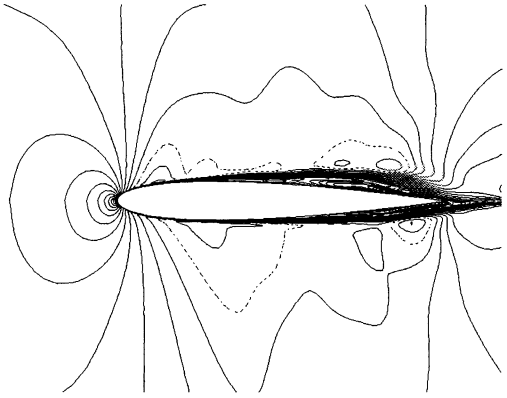

Figure 5: Instantaneous Mach iso-contours for a Reynolds number of $3 \cdot 10^5$. The sonic line (dashed line) is depicted.

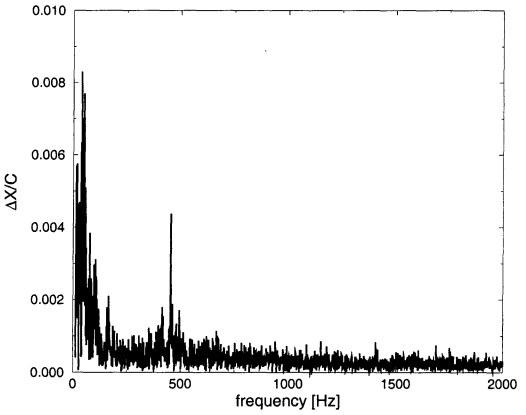

Figure 6: Fast Fourier Transform of the shock movements for a Reynolds number of $5 \cdot 10^5$.

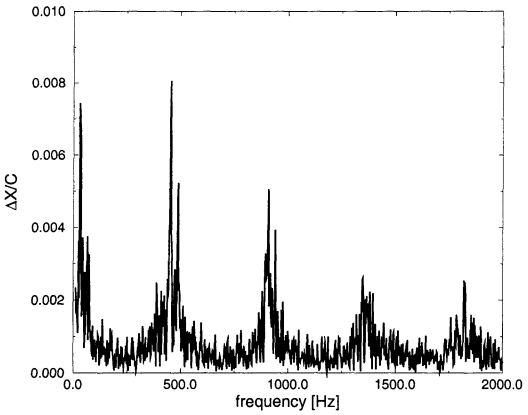

Figure 7: Fast Fourier Transform of the shock movements for a Reynolds number of $1 \cdot 10^6$.

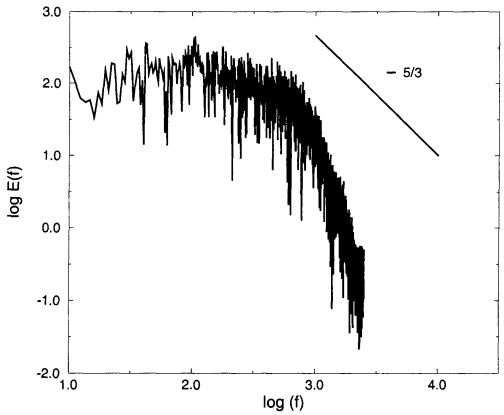

Figure 10: Kinetic energy spectrum of the fluctuations at X/C=0.60 for a Reynolds number of $5 \cdot 10^5$. The Kolmogorov -5/3 decay is depicted.

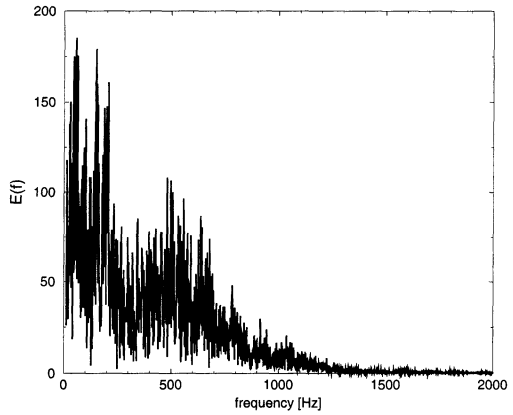

Figure 8: Kinetic energy spectrum of the fluctuations at X/C=0.50 for a Reynolds number of $5 \cdot 10^5$.

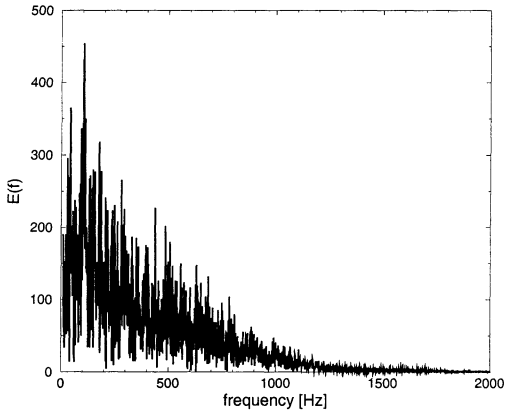

Figure 9: Kinetic energy spectrum of the fluctuations at X/C=0.60 for a Reynolds number of $5 \cdot 10^5$.